AFRL-AFOSR-VA-TR-2016-0055

Coupling photonics and coherent spintronics for low-loss flexible optical logic

Jesse Berezovsky
CASE WESTERN RESERVE UNIV CLEVELAND OH

12/02/2015
Final Report

Air Force Research Laboratory
AF Office Of Scientific Research (AFOSR)/ RTA1
Arlington, Virginia 22203
Air Force Materiel Command

REPORT DOCUMENTATION PAGE

Form Approved
OMB No. 0704-0188

1. REPORT DATE *(DD-MM-YYYY)*	2. REPORT TYPE	3. DATES COVERED *(From - To)*
19-11-2015	Final report	15/06/2012 - 14/06/2015

4. TITLE AND SUBTITLE
Coupling photonics and coherent spintronics for low-loss flexible optical logic

5a. CONTRACT NUMBER

5b. GRANT NUMBER
FA9550-12-1-0277

5c. PROGRAM ELEMENT NUMBER

6. AUTHOR(S)
Jesse Berezovsky

5d. PROJECT NUMBER

5e. TASK NUMBER

5f. WORK UNIT NUMBER

7. PERFORMING ORGANIZATION NAME(S) AND ADDRESS(ES)
Case Western Reserve University
10900 Euclid Ave.
Cleveland, OH 44106-1712

8. PERFORMING ORGANIZATION REPORT NUMBER

9. SPONSORING/MONITORING AGENCY NAME(S) AND ADDRESS(ES)
AF OFFICE OF SCIENTIFIC RESEARCH
875 NORTH RANDOLPH STREET, RM 3112 ARLINGTON VA 22203

10. SPONSOR/MONITOR'S ACRONYM(S)
AFOSR

11. SPONSOR/MONITOR'S REPORT NUMBER(S)

12. DISTRIBUTION/AVAILABILITY STATEMENT
Approved for public release.

13. SUPPLEMENTARY NOTES

14. ABSTRACT
Over the course of this project, we have made advances in several key areas: 1. Controlling spin-photon interactions using narrow-linewidth optical signals. We achieved the optimal balance between the competing needs for high speed and narrow linewidth by modulating a narrow-linewidth laser with only the frequency components needs for interaction with coherent spin dynamics. 2. Understanding fundamental spin-photon interactions in semiconductor nanocrystals. We studied the initialization and evolution of coherent spin states at room temperature, yielding a guide towards possible applications. These results were compared to theory to provide a detailed understanding of spin pumping, dynamics, and decoherence in these structures. 3. Integration of semiconductor nanocrystals in photonic systems for enhanced spin-photon interaction. We have taken a multi-pronged approach to exploring possible systems for enhancing interactions between light and spins, and integrating these systems into devices, ranging from macroscopic optical cavities, to arrays of microlens cavities, to quantum dot-impregnated integrated polymer waveguides.

15. SUBJECT TERMS
Photonic devices, spintronics, optical signal processing

16. SECURITY CLASSIFICATION OF:			17. LIMITATION OF ABSTRACT	18. NUMBER OF PAGES	19a. NAME OF RESPONSIBLE PERSON
a. REPORT	b. ABSTRACT	c. THIS PAGE			Jesse Berezovsky
U	U	U	UU	12	19b. TELEPHONE NUMBER *(Include area code)* 216-368-4034

Reset

INSTRUCTIONS FOR COMPLETING SF 298

1. REPORT DATE. Full publication date, including day, month, if available. Must cite at least the year and be Year 2000 compliant, e.g. 30-06-1998; xx-06-1998; xx-xx-1998.

2. REPORT TYPE. State the type of report, such as final, technical, interim, memorandum, master's thesis, progress, quarterly, research, special, group study, etc.

3. DATES COVERED. Indicate the time during which the work was performed and the report was written, e.g., Jun 1997 - Jun 1998; 1-10 Jun 1996; May - Nov 1998; Nov 1998.

4. TITLE. Enter title and subtitle with volume number and part number, if applicable. On classified documents, enter the title classification in parentheses.

5a. CONTRACT NUMBER. Enter all contract numbers as they appear in the report, e.g. F33615-86-C-5169.

5b. GRANT NUMBER. Enter all grant numbers as they appear in the report, e.g. AFOSR-82-1234.

5c. PROGRAM ELEMENT NUMBER. Enter all program element numbers as they appear in the report, e.g. 61101A.

5d. PROJECT NUMBER. Enter all project numbers as they appear in the report, e.g. 1F665702D1257; ILIR.

5e. TASK NUMBER. Enter all task numbers as they appear in the report, e.g. 05; RF0330201; T4112.

5f. WORK UNIT NUMBER. Enter all work unit numbers as they appear in the report, e.g. 001; AFAPL30480105.

6. AUTHOR(S). Enter name(s) of person(s) responsible for writing the report, performing the research, or credited with the content of the report. The form of entry is the last name, first name, middle initial, and additional qualifiers separated by commas, e.g. Smith, Richard, J, Jr.

7. PERFORMING ORGANIZATION NAME(S) AND ADDRESS(ES). Self-explanatory.

8. PERFORMING ORGANIZATION REPORT NUMBER. Enter all unique alphanumeric report numbers assigned by the performing organization, e.g. BRL-1234; AFWL-TR-85-4017-Vol-21-PT-2.

9. SPONSORING/MONITORING AGENCY NAME(S) AND ADDRESS(ES). Enter the name and address of the organization(s) financially responsible for and monitoring the work.

10. SPONSOR/MONITOR'S ACRONYM(S). Enter, if available, e.g. BRL, ARDEC, NADC.

11. SPONSOR/MONITOR'S REPORT NUMBER(S). Enter report number as assigned by the sponsoring/ monitoring agency, if available, e.g. BRL-TR-829; -215.

12. DISTRIBUTION/AVAILABILITY STATEMENT. Use agency-mandated availability statements to indicate the public availability or distribution limitations of the report. If additional limitations/ restrictions or special markings are indicated, follow agency authorization procedures, e.g. RD/FRD, PROPIN, ITAR, etc. Include copyright information.

13. SUPPLEMENTARY NOTES. Enter information not included elsewhere such as: prepared in cooperation with; translation of; report supersedes; old edition number, etc.

14. ABSTRACT. A brief (approximately 200 words) factual summary of the most significant information.

15. SUBJECT TERMS. Key words or phrases identifying major concepts in the report.

16. SECURITY CLASSIFICATION. Enter security classification in accordance with security classification regulations, e.g. U, C, S, etc. If this form contains classified information, stamp classification level on the top and bottom of this page.

17. LIMITATION OF ABSTRACT. This block must be completed to assign a distribution limitation to the abstract. Enter UU (Unclassified Unlimited) or SAR (Same as Report). An entry in this block is necessary if the abstract is to be limited.

Final report for FA9550-12-1-0277:
"Coupling photonics and coherent spintronics for low-loss flexible optical logic"

PI: Jesse Berezovsky, Case Western Reserve University

The motivation of this project was to understand and control the interaction between light and coherent spins in semiconductor nanocrystal quantum dots (NCQDs), with the particular aim of enabling spin-mediated optical signal processing devices. The off-resonant nature of these spin-based phenomena allow optical logic operations that are, in principle, lossless. Furthermore, the electron spins that mediate the optical logic may also be addressed electrically or magnetically, allowing for hybrid systems incorporating optical computing, standard electronics, and magnetic memory. The ability to perform communication, logic, and memory in a hybrid system enables the compact and high-speed technology required for future needs.

Much of the work here was carried out by one recently-graduated PhD student supported by this program, Ahmad Fumani, with assistance from the PI. Undergraduate researchers also contributed to the work, including Johnathon Frey, Jeffery Oleski, Tadeas Liska, and Joseph Szabo.

Over the course of this project, we have made advances in several key areas: 1. Controlling spin-photon interactions using narrow-linewidth optical signals, 2. Understanding fundamental spin-photon interactions in semiconductor nanocrystals, and 3. Integration of semiconductor nanocrystals in photonic systems for enhanced spin-photon interaction.

1. Controlling spin-photon interactions using narrow-linewidth optical signals:

Conventional methods for controlling interactions between light and coherently-evolving spins in semiconductor nanocrystals require complex ultra-fast, spectrally-broad pulsed laser systems which will be difficult to combine with integrated devices. Therefore, we wish to develop an interface between coherent spins and light that uses narrow-linewidth CW lasers as a source.

To this end, we developed a technique, which we refer to as Fourier-transform spin resonance (FTSR), which was the subject of a paper published in August 2012 [1]. The setup used for FTSR measurements is shown in Fig. 1(a). Whereas the more traditional time-resolved FR setup (see Fig. 2(a)) relies on a pulsed supercontinuum fiber laser (~$100,000), the FTSR setup is based on a pair of off-the-shelf laser diodes (~$20 each). In principle, the two measurements provide the same information. (For experimental purposes, however, the time resolved FR measurements are more flexible and easier to interpret, and thus are still used for studying coherent spin dynamics.) For FTSR measurements, the pump and probe lasers are driven by an RF signal at frequency Ω combined with a DC bias modulated

at low frequencies f_1 and f_2. The modulation at f_1 and f_2 allow for lock-in based detection. The pump and probe lasers are then used for a Faraday rotation measurement in the same way as in the time-resolved Faraday rotation measurements.

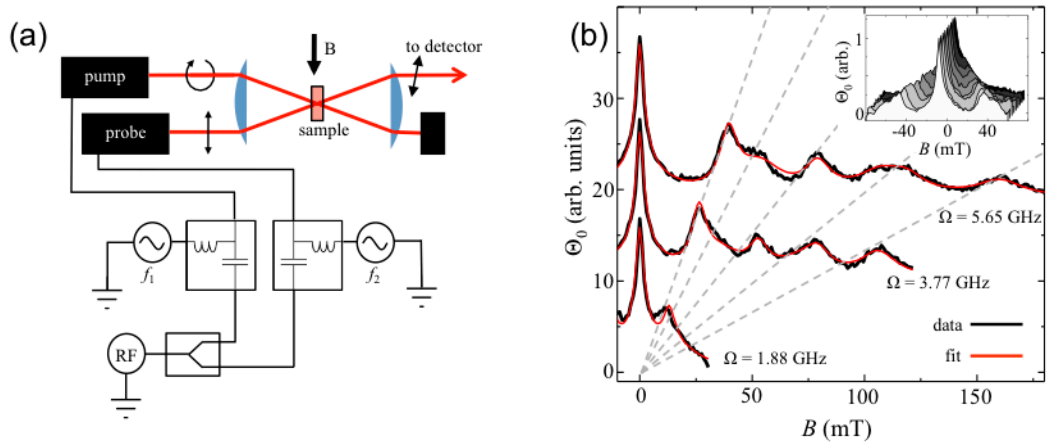

Figure 1. Probing spin dynamics using narrow linewidth lasers. (a) Setup for Fourier transform spin resonance (FTSR) measurement. (b) FTSR data (black) and fits (red) from an ensemble of room- temperature NCQDs.

The FTSR measurement works by producing a signal only when the modulation frequency Ω is resonant with a component of the spin dynamics. By sweeping Ω, FTSR produces the Fourier transform of the spin dynamics. (The real and imaginary parts of the Fourier transform are obtained by changing the relative phase of the pump and probe modulation.) Alternatively, by fixing Ω and sweeping a magnetic field B, one maps the evolution of the Ω-component of the spin dynamics as a function of B.

Figure 1(b) shows FTSR measurements vs. B, at three values of Ω from an ensemble of room temperature NCQDs. The resonances shift to higher B with increasing Ω. The first two resonances at $\Omega > 0$ correspond to the two distinct components present in NCQD samples. Subsequent peaks arise from higher harmonics of these two frequencies. The inset shows additional curves at more values of Ω, illustrating how the peaks shift with Ω.

By fitting the FTSR data to a model function, we can obtain information about the coherent evolution of spins in the sample. Fits are shown in red in Fig. 1(b). The fits reveal g-factors, spin lifetimes, and inhomgeneous dephasing effects in agreement with results from time-resolved FR measurements.

The FTSR approach described above is a continuous wave measurement, averaged over time. For optical signal processing, the optical signals should be as short as possible. Ultrafast pulses are too short in that they necessarily involve large linewidths, so we have explored modulated, narrow-linewidth lasers to tailor pulse lengths to optimize fast operation and narrow linewidth. We have used an electro-

optic modulator, synchronized with the pulsed pump laser, to measure spins in QDs using 10-ns-duration, narrow linewidth probe pulses. Data from such an experiment is shown in Fig. 6(b). Since the 10-ns-long pulse is longer than the spin lifetime in the QDs, the signal measured is the time-average of the spin dynamics resulting from the pump pulse. At zero magnetic field, this signal is a maximum. By increasing the magnetic field, the interaction is turned off. The amplitude of the interaction is fairly small (~30 μrad), though shorter, higher power pulses will improve this, as will ultimately, integration with resonators. The next step would be to combine this pulsed measurement with the FTSR modulation for fast, narrow-linewidth measurement, with frequency resolution.

2. Understanding fundamental spin-photon interactions in semiconductor nanocrystals:

In order to use spins in nanocrystal quantum dots (NCQDs) as an active medium for controlling optical signals, we must gain a better understanding of the underlying processes that govern decoherence and decay of spin states in these structures. We performed a detailed series of time-resolved Faraday rotation measurements on room-temperature ensembles of NCQDs, and developed a technique for reliably extracting information about spin dephasing and decoherence from the resulting dataset. These results were published in Physical Review B as an Editor's Suggestion [2].

Figure 2(a) shows the setup that we have built and employed for two-color time-resolved Faraday rotation measurements. The pump and probe pulses are provided by a supercontinuum fiber laser with two sets of motorized variable edgepass filters, allowing us to select the center wavelength and bandwidth of both the pulse trains. The pump pulses are reflected off of a movable retroreflector, yielding controllable time delay between the pump and probe. The pump is circularly polarized to excite spin-polarized electrons into the conduction band of the NCQDs. The probe, arriving at the sample a time Δt after the pump, is linearly polarized to measure the spin projection in the sample via the Faraday effect. The sample in this case is an ensemble of ~6-nm-diameter CdSe NCQDs, either in solution, or on a substrate in a polymer matrix.

By sweeping the time delay between the pump and probe, we obtain the projection of the ensemble spin along the probe propagation direction as a function of time, as shown in Fig. 2(b). Here, the pump arrives at time $t = 0$, initializing the spin and giving rise to the sharp jump in the FR signal. A transverse magnetic field $B = 200$ mT is applied, causing the spins to coherently precess, which is seen as oscillations of the FR signal. The signal then decays away with a time constant ~1 ns. It is important to gain an understanding of what processes give rise to the decay of the spin signal seen in Fig. 2(b). Extracting precise and reliable information about the spin decay from the data in Fig. 2(b) requires accurate fitting of the data to a model function – a task which is complicated by several factors. First, there are two

distinct components to the observed dynamics, with different precession frequencies and decay characteristics (this can be seen as beating in the zoomed-in inset in Fig. 2(b)). These two components must be captured by separate terms in the fitting function. Second, the decay profile of each component is not a simple exponential decay. Therefore, to obtain meaningful fits, we must develop a theory that captures the actual decay profile. Third, with two separate precessing and decaying components, the number of parameters in the model becomes large. Thus when fitting, we must proceed carefully to ensure that the results are meaningful.

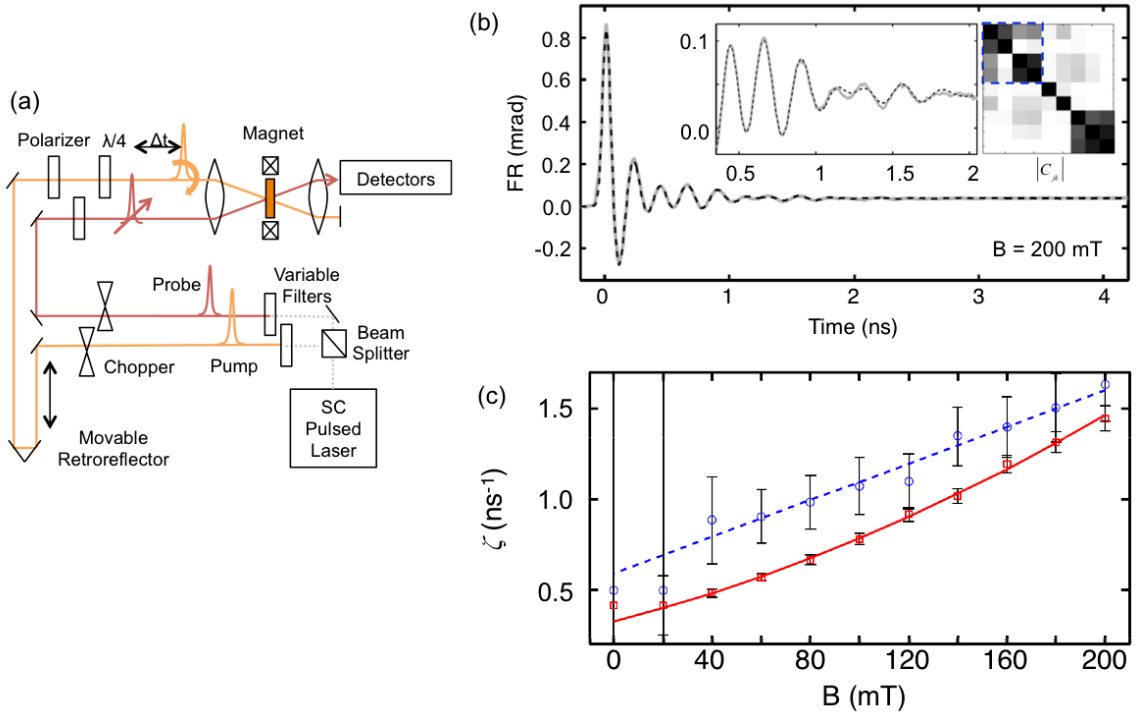

Figure 2. Studying room-temperature dephasing and decoherence in NCQDs. (a) Setup for two-color time-resolved Faraday rotation measurement. (b) Typical FR data (gray) with fit to model function (black dashed). Left inset: zoom-in on data and fit. Right inset: Absolute value of cross-correlation matrix |C|. (c) Total spin decay rate ζ vs. magnetic field *B* for the two coherent spin components. One component is well-fit by a linear function, the other by a quadratic function.

We have developed a model of spin decoherence and dephasing in NCQDs that captures the observed decay of the spin signal. The black dashed line in in Fig. 2(b) is a fit using this model to the data shown in gray. The zoomed-in inset shows the data and fit at later times. Models used in previous work have included inhomogeneous dephasing and an exponential decoherence term. To make these models agree with the data, however, it is necessary to exclude the data at early times (t < 200 ps). This arbitrary exclusion of data leads to unreliable fit results. We have described another spin decoherence mechanism, which we call fine-structure decoherence (FSD), which arises from rapid transitions between the fine-structure states of the exciton in the NCQD. When including FSD in the model function, all data in the dataset are well-described by the model at all times.

In order to deal with the large number of parameters in the model, we not only study the best-fit curve, but also the cross-correlation matrix **C** of the fit parameters. The absolute value of the cross-correlation matrix |**C**| is shown in as the second inset in Fig. 2(b). Here, each row and column corresponds to a particular parameter in the model, and black indicates complete correlation, and white indicates complete lack of correlation. Ideally, a fit function would have minimal cross-correlations – that is, black on the diagonal and white everywhere else. If one naively constructs the fit function, large regions of the matrix are highly correlated. We have recast the model function and fixed parameters that cannot be determined to reduce cross-correlations between the parameters that govern the spin decay characteristics (those inside the dashed box in the inset to Fig. 2(b)).

By fitting FR data at different magnetic fields *B*, we can extract the characteristic decay rate ζ for both components of the signal vs. B (Fig. 2(c)). The error bars here result from residual cross-correlation between fit parameters. The decay rate for one component is well-fit by a linear function, but the other component require a second-order polynomial to achieve a good fit. In our model, the y-intercept of these curves indicates the magnetic-field-independent exponential decoherence, the linear slope arises from inhomogeneous dephasing, and the quadratic component is due to the FSD mechanism. This allows us to independently measure the contributions of these different mechanisms to the total decay behavior.
The procedure for measuring spin decay mechanisms presented above will now allow us to study how these mechanisms vary in different types of structures and environments, and give clues about how to control them.

A key capability for future spin-based photonic devices is to optically initialize spins in NCQDs at room temperature. Though it has been known for about 15 years that such pumping is possible, there had been no study of the process, or of how to optimize it. To investigate this, we have carried out a series of time-resolved Faraday rotation measurements as a function of the excitation energy. The magnitude of the resulting signal yields a measure of the spin pumping efficiency. These measurements were repeated on three ensembles of NCQDs, with different mean diameter. We have found that all samples showed a maximum spin pumping efficiency resonant with the lowest energy transition, but only the largest size showed a second peak at higher energy. This will be useful for future experiments and applications, in that it permits efficient spin pumping away from the resonant transition. These results [3,4], in conjunction with the results on spin dephasing and decoherence in these structures [2], provide a solid foundation for using these effects in spintronic/photonic devices.

To collect data on spin pumping efficiency, we used our time-resolved Faraday rotation experiment, with its flexible wavelength tuning capabilities. For these measurements, we fix the probe wavelength at an optimal value, and scan the pump wavelength from 460 to 690 nm. At each pump wavelength, a time-resolved

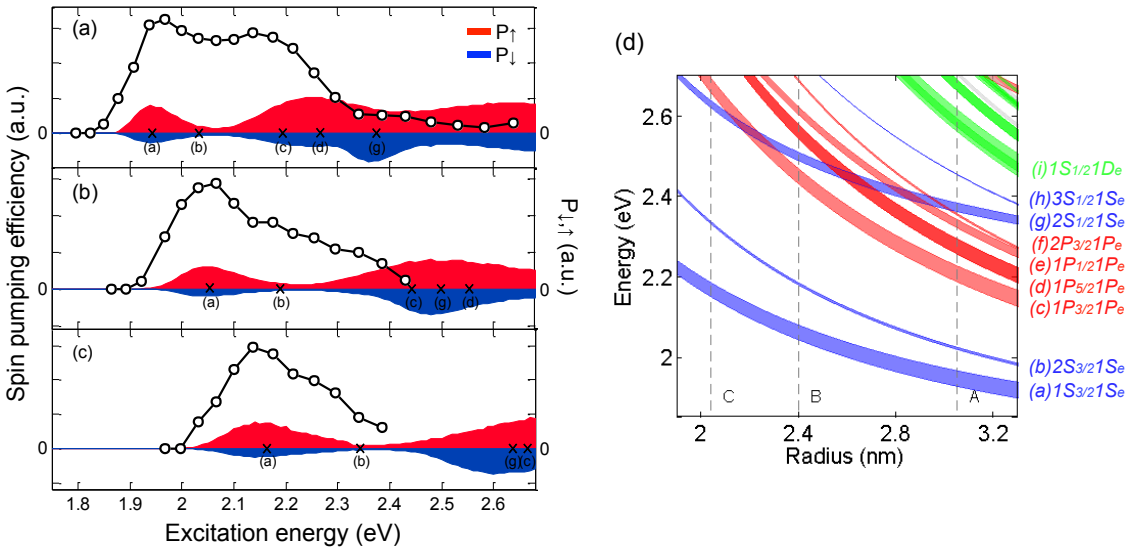

Figure 3. Spin pumping efficiency in nanocrystal quantum dots. (a)-(c) Measured spin pumping efficiency vs. excitation energy in samples A-C (black circles). Red indicates calculated oscillator strength for spin up electrons, blue for spin down electrons. (d) Calculated spectrum of optical transitions vs. particle size. Width of lines indicates oscillator strength.

Faraday rotation trace is collected, and the magnitude of the signal provides a measure of the spin pumping efficiency. Three samples were measured, with mean particle radius 3.1, 2.4, and 2.1 nm, referred to as sample A, B, and C respectively.

Figure 3 (a)-(c) shows the measured spin pumping efficiency vs. excitation energy for the three samples A-C (black circles). As expected, the data is shifted upwards in energy for smaller sizes, because increasing quantum confinement increases the energy of the optical transitions. The largest sample (A) shows two nearly equal peaks in the spin pumping efficiency. As the QD size is decreased, the second peak disappears.

To understand the observed spin pumping behavior, we have carried out calculations of the quantum-confined states in these structures, and determined the spin dependent oscillator strengths of the relevant transitions. We first used a simple effective mass approximation to calculate the electron and hole wavefunctions and energies in the conduction band and three valence sub-bands (heavy hole, light hole, and split-off hole). With these wavefunctions, we can calculate oscillator strengths for transitions from valence band to conduction band states, in the envelope function approximation. The resulting transition energies are shown in Fig. 3(d) vs. QD radius, with the width of the line indicating the oscillator strength of that transition. The mean radii in the three samples are

indicated. The valence band states are generally superpositions of the three valence subbands. Due to angular momentum selection rules, circularly polarized excitation generates different conduction band spin states from different valence sub-bands. We can separate the oscillator strengths from the different valence sub-bands to find the degree of conduction band spin polarization generated when driving each transition. The results of this calculation are shown as the red and blue regions in Fig. 3 (a)-(c). Red indicates the amplitude for spin up generation, whereas blue indicates the amplitude for spin down generation. The width of the features arises from the distribution of QD size within the ensemble. The difference between the red and blue amplitude is proportional to the expected spin pumping efficiency. The key finding here is the importance of transition (g) which crosses a number of other transitions in the size range studied here. This transition is significant in that it is the lowest energy transition to be dominated by the light hole and split off hole bands, which excite spins polarized in the opposite direction to transitions from the heavy-hole band. When this transition is excited, it dramatically reduces the spin pumping efficiency. In all samples, the first peak in spin pumping efficiency arises from transitions (a) and (b). In sample A, the second peak is from (c)-(f). As the quantum dots become smaller, the transitions change ordering so that transition (g) appears at lower energy than (c)-(f), so the reduction in spin pumping from transition (g) kills off the second peak.

These results will play an important role in ongoing efforts to engineer useful spin-photon interactions in these materials. In designing experiments and potential devices, we now have guidelines for choosing the correct QD size, and excitation energy. It is particularly useful that larger QDs permit strong spin pumping at higher energies, allowing different energies to be used for excitation and measurement.

3. Towards integrated devices and enhancement of spin-photon interactions with optical cavities

Our approach to enhancing spin-photon interactions to the point where they can be used to implement logic operations had two focuses. First, we planned to study these interactions in a highly controllable system of NCQDs in solution within a macroscopic Fabry-Pérot resonator. Second, we have created integrated optical resonators coupled to deposited NCQDs.

We constructed an experimental platform for studying spin-photon interactions in a macroscopic Fabry-Pérot resonator. A photograph is shown in Fig. 4(a). The cavity consists of two plano-concave partially reflective dielectric mirrors with designed reflectivity R = 95%. The mirrors are held in positioning stages with a separation of twice their focal lengths. This produces a confocal optical cavity, with a focus at the center of the cavity. One of the mirrors is mounted on a piezo-electric actuator which allows for fine tuning of the cavity length. The mirrors are supported by a solid Invar base to reduce vibration and thermal drift. We can then insert a cell containing NCQDs in solution at the focus of the cavity. The cells are commercially

available quartz cells with optical path length ranging from 50 to 500 microns. We have obtained a size series of these cells and deposited onto them an anti-reflection coating, so as to not introduce extra loss in the cavity. A stabilized HeNe laser is coupled into one mirror, and the transmission is monitored via a photodiode. Measurements can be taken either by sweeping the piezo voltage to scan the cavity length through a resonance, or by using feedback control on the piezo voltage to keep the cavity at a fixed position on a resonance.

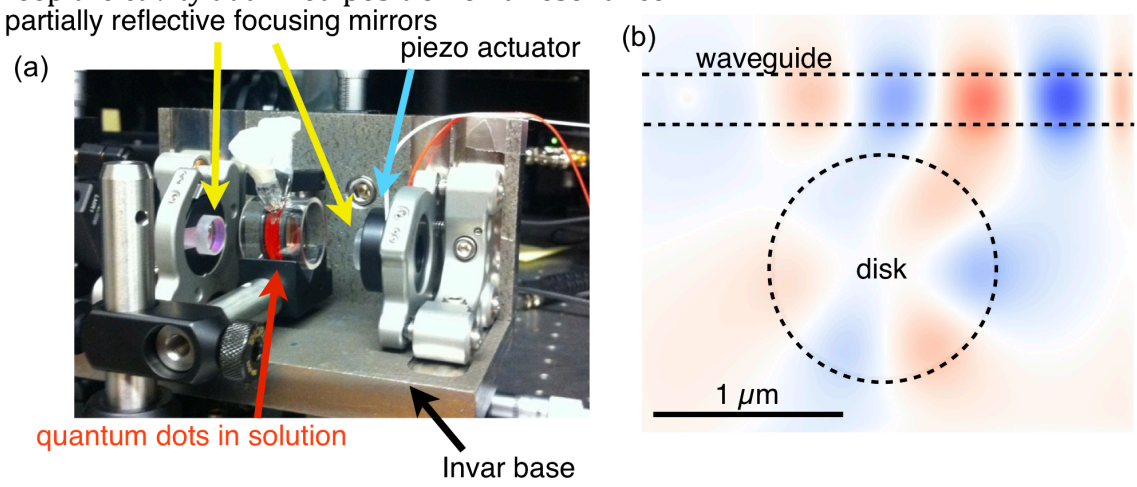

Figure 4. Enhancing spin-photon interactions with optical cavities. (a) Photograph of confocal Fabry-Pérot resonator with NCQDs in solution at the focal point. (b) Finite-difference time domain simulation of a silicon nitride microdisk resonator coupled to an optical waveguide.

Initial results have indicated a cavity finesse $F \approx 25$ with no NCQD cell in the cavity. This is close to the expected finesse, and could likely be increased with higher reflectivity mirrors. With a quantum dot cell in the cavity (as shown in Fig. 3(a)), the finesse is reduced to $F \approx 22$. The excitation of spins in the NCQDs using a pump laser is challenging due to the experimental geometry, and requirements of the cavity, and is still an ongoing effort. This will then allow us to observe the effects of the cavity on the Faraday effect.

We have also explored a simple technique for enhancing spin-dependent polarization rotation, which is to partially polarize light using a series of Brewster reflectors (BRs). In the proper geometry, these can be used to reduce the un-rotated component of light that has interacted with one or more spins, thereby increasing the rotation angle. By changing the number of BRs, the rotation angle can be increased, allowing one to find the configuration that optimizes rotation angle and signal-to-noise ratio (SNR) for a particular application (see Fig. 7(a) and (b)).

In parallel with the macroscopic cavities, we have designed and fabricated initial integrated cavities coupled to NCQDs. In order to design these systems, we have performed simulations both using transfer matrix calculations and using finite-difference time domain (FDTD) simulation. Fig. 4(b) shows an example result from an FDTD simulation of a silicon nitride microdisk resonator coupled to a waveguide.

The red and blue indicate electric field intensity at a particular time. NCQDs would then be deposited by drop casting, or by spin- coating and/or patterning of a polymer film.

In order to incorporate colloidal quantum dots in integrated devices, we will need methods for depositing the colloidally-dispersed quantum dots onto substrates. Previous measurements have mainly been performed on QDs in solution, or dispersed in a thick polymer film. The quantum dot films required for future devices must have thickness on the order of 100 nm, must be uniform, with minimal optical scattering, yet still have sufficient optical density to provide strong spin-photon interactions. Such films may be directly deposited onto integrated photonic devices, or built into low mode-volume optical cavities.

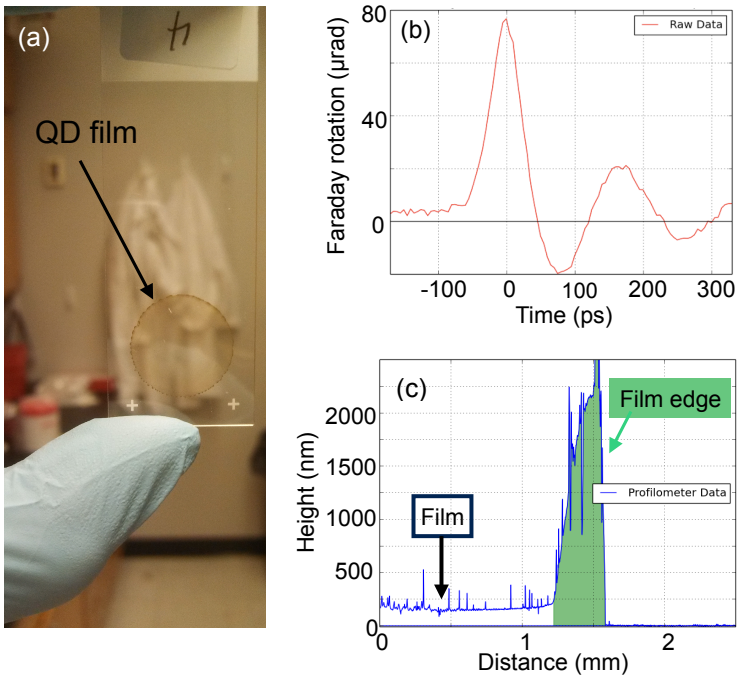

Figure 5. (a) Photograph of 150-nm-thick quantum dot film. (b) Faraday rotation data from film shown in (a), showing coherent spin precession in a magnetic field. (c) Height profile of film shown in (a).

Producing QD films that meet our requirements involves choosing the correct solvents and deposition conditions. Deposition of films by drop casting from the as-grown solution and evaporating in ambient conditions results in the "coffee-stain" effect, where QDs aggregate in concentric rings as the solvent evaporates. These films are highly nonuniform, and scatter light strongly. In contrast, changing solvents can reduce this effect. Figure 5(a) shows a photograph of a QD film which is uniform over the central area and optically smooth. This film was synthesized by dispersing dried CdSe/ZnS core/shell quantum dots in 10% octane, 90% hexane solution. These solutions were then drop cast on a glass substrate and the allowed to evaporate under ambient temperature and pressure. This particular solution counteracts particle aggregation (coffee stain effect) on the outside of the droplet by allowing the QDs to more uniformly drop out of solution across the entire area of the droplet. The volatile alkanes induce recirculation in the droplet so more uniform samples can be made. Adding a second, lighter volatile solvent (hexane) increases evaporation time and destabilizes the quantum dots in solution, further increasing deposition uniformity. Additionally, the evaporation may be carried out in a 2-propanol vapor environment, which also counteracts coffee-stain effects.

We measure spin-photon interaction in these QD films using a time-resolved Faraday rotation measurement (Fig. 5b). We obtain clear signal-to-noise on this 150-nm-thick film (thickness measurement shown Fig. 5c), and a maximum rotation angle of about 80 μrad. This is only about 10 times less the signal obtained from QDs in solution in a 1-mm thick cuvette, despite a ~5000-fold reduction in thickness. The ideal degree of rotation would be ~1 rad, requiring an enhancement of about 10^4. These thin films with minimal scattering will permit integration with high quality optical cavities, which may be capable of providing this level of interaction enhancement.

We have made progress on implementation of integrated photonic devices for exploring spin-photon coupling. We have fabricated silicon nitride structures on top of silicon dioxide, using electron beam lithography and plasma etching. Typical structures are shown in Figure 6(a). These consist of a 50 μm long waveguide, with grating couplers on either end. Input and output light will be focused/collected from the grating couplers via a microscope objective. Currently, we are working on improving side-wall characteristics (roughness and slope), and optimizing the grating couplers. Initially, we plan to deposit QD films on these structures and measure the resulting coupling by monitoring waveguide transmission as the QDs are pumped. We also plan to fabricate these structures onto scanned cantilevers to measure interactions with single QDs, in conjunction with another ongoing project. The next step will be to fabricate integrated photonic resonators to study how the interactions can be enhanced.

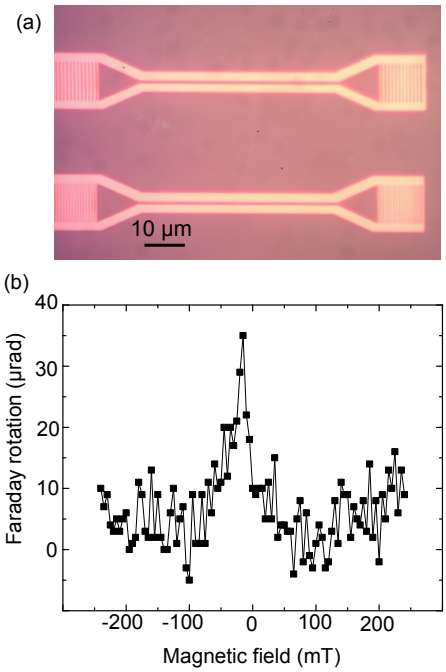

Figure 6. (a) Silicon nitride waveguides with grating couplers. (b) Faraday rotation vs. magnetic field measured using 10 ns, narrow linewidth pulses.

Optical waveguides and resonators are essential components of integrated optical devices. We have developed a fabrication method for NCQD-polymer composite optical waveguides. The optical medium of the waveguide is made of a PMMA and NCQD composite. It is fabricated via electron-beam lithography on a thin film of Cytop, an optical Fluoropolymer resin with refractive index of ~ 1.34, atop a silicon substrate. An optical micrograph of a polymer waveguide is shown in Fig. 7(e). We have characterized the transmission properties of these waveguides with different cross-sections and NCQD concentrations. The next step will be to explore spin-based measurements with optical signals traveling through the waveguides.

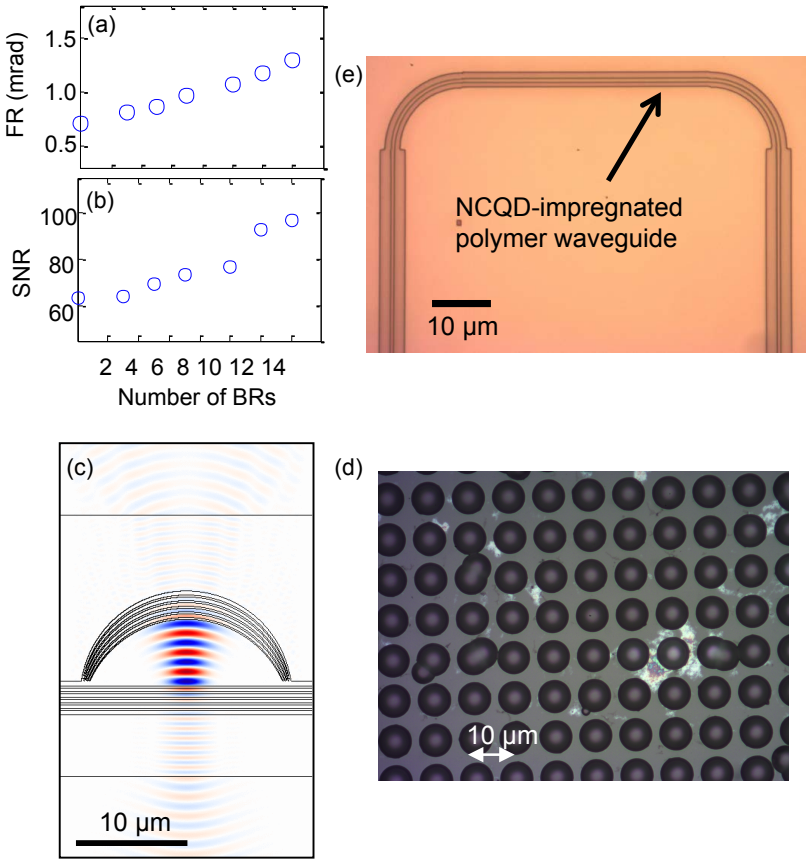

Figure 7. (a) Enhancement of FR signal and (b) signal-to-noise ratio (SNR) by a series of Brewster reflectors (BRs). (c) FDTD simulation of microlens cavity. (d) Microlens reflector array. (e) NCQD-impregnated polymer waveguide.

A key component of this work involves enhancing the interactions between spins and photons. In some cases, this may be accomplished on-chip, with integrated resonators. However, some steps for the proposed applications would be more easily accomplished via free-space optical interactions. (i.e. focusing laser pulses onto the device through free space). For this purpose, we have developed a platform for enhancing these interactions with arrays of patterned low-mode-volume cavities. Figure 7(c) shows a simulation of one of these micro-cavities in cross-section. The cavity consists of two distributed Bragg reflectors. The bottom DBR is planar, while the top DBR has hemispherical depressions formed by performing an isotropic etch through a nanoscale pinhole mask. Input light focused on this microlens cavity is confined to a small volume inside (red and blue). Figure 7(d) shows an optical microscope image of an array of microlenses. These consist of hemispherical depressions etched into quartz, and coated with a DBR stack. The active layer containing a film of NCQDs is fabricated on top of a planar reflector. The reflector with the microlenses is then placed atop the active layer, with separation controlled by a piezoelectric actuator. Optical signals to operate on the spins are then incident on the structure from the top, focused into the microlens cavities.

Conclusions:

The progress made over the course of this project provides a basis for beginning to engineer photonic devices that incorporate coherent spin-based functionality at room temperature. The fundamental understanding of optical spin pumping, and coherent dynamics in NCQDs at room temperature provide a guide to the appropriate nanostructures for these applications. The exploration of techniques for coupling light and spins reveals the opportunities and challenges for doing so in practical integrated devices. Finally, we have taken a multi-pronged approach to developing platforms for enhancement of spin-photon interactions, and on-chip integration. Going forward, building off of these platforms will allow us to realize the potential of spin-based photonic devices.

Publications:

[1] J. A. Frey and J. Berezovsky, Frequency-domain optical probing of coherent spins in nanocrystal quantum dots. *Optics Express* 20:20011, Aug. 2012. http://dx.doi.org/10.1364/OE.20.020011

[2] Fumani, A. Khastehdel, and J. Berezovsky. "Magnetic-field-dependent spin decoherence and dephasing in room-temperature CdSe nanocrystal quantum dots." *Physical Review B* 88.15 (2013): 155316. (Editor's Suggestion)
DOI: http://dx.doi.org/10.1103/PhysRevB.88.155316

[3] Fumani, A. K., & Berezovsky, J. Spin-Pumping Efficiency in Room-Temperature CdSe Nanocrystal Quantum Dots. *The Journal of Physical Chemistry C*, *118*(48), (2014): 28202-28206.

[4] Berezovsky, J., Fumani, A. K., & Wolf, M. Room-temperature initialization, dynamics, and measurement of coherent electron spins in strongly confined quantum dots. In *SPIE NanoScience+ Engineering* (pp. 916707-916707). International Society for Optics and Photonics (2014).

1.

1. Report Type

Final Report

Primary Contact E-mail
Contact email if there is a problem with the report.

jab298@case.edu

Primary Contact Phone Number
Contact phone number if there is a problem with the report

2163684034

Organization / Institution name

Case Western Reserve University

Grant/Contract Title
The full title of the funded effort.

Coupling photonics and coherent spintronics for low-loss flexible optical logic

Grant/Contract Number
AFOSR assigned control number. It must begin with "FA9550" or "F49620" or "FA2386".

FA9550-12-1-0277

Principal Investigator Name
The full name of the principal investigator on the grant or contract.

Jesse Berezovsky

Program Manager
The AFOSR Program Manager currently assigned to the award

Gernot Pomrenke

Reporting Period Start Date

06/15/2012

Reporting Period End Date

06/14/2015

Abstract

The motivation of this project was to understand and control the interaction between light and coherent spins in semiconductor nanocrystal quantum dots (NCQDs), with the particular aim of enabling spin-mediated optical signal processing devices. The off-resonant nature of these spin-based phenomena allow optical logic operations that are, in principle, lossless. Furthermore, the electron spins that mediate the optical logic may also be addressed electrically or magnetically, allowing for hybrid systems incorporating optical computing, standard electronics, and magnetic memory. The ability to perform communication, logic, and memory in a hybrid system enables the compact and high-speed technology required for future needs.

Over the course of this project, we have made advances in several key areas: 1. Controlling spin-photon interactions using narrow-linewidth optical signals. We achieved the optimal balance between the competing needs for high speed and narrow linewidth by modulating a narrow-linewidth laser with only the frequency components needs for interaction with coherent spin dynamics. 2. Understanding fundamental spin-photon interactions in semiconductor nanocrystals. We studied the initialization and evolution of coherent spin states at room temperature, yielding a guide towards possible applications. These results were compared to theory to provide a detailed understanding of spin pumping, dynamics, and

decoherence in these structures. 3. Integration of semiconductor nanocrystals in photonic systems for enhanced spin-photon interaction. We have taken a multi-pronged approach to exploring possible systems for enhancing interactions between light and spins, and integrating these systems into devices, ranging from macroscopic optical cavities, to arrays of microlens cavities, to quantum dot-impregnated integrated polymer waveguides.

Distribution Statement

This is block 12 on the SF298 form.

Distribution A - Approved for Public Release

Explanation for Distribution Statement

If this is not approved for public release, please provide a short explanation. E.g., contains proprietary information.

SF298 Form

Please attach your SF298 form. A blank SF298 can be found here. Please do not password protect or secure the PDF The maximum file size for an SF298 is 50MB.

AFD-070820-035.pdf

Upload the Report Document. File must be a PDF. Please do not password protect or secure the PDF . The maximum file size for the Report Document is 50MB.

AFOSR_final_report_Berezovsky.pdf

Upload a Report Document, if any. The maximum file size for the Report Document is 50MB.

Archival Publications (published) during reporting period:

[1] J. A. Frey and J. Berezovsky, Frequency-domain optical probing of coherent spins in nanocrystal quantum dots. Optics Express 20:20011, Aug. 2012. http://dx.doi.org/10.1364/OE.20.020011

[2] Fumani, A. Khastehdel, and J. Berezovsky. "Magnetic-field-dependent spin decoherence and dephasing in room-temperature CdSe nanocrystal quantum dots." Physical Review B 88.15 (2013): 155316. (Editor's Suggestion)
DOI: http://dx.doi.org/10.1103/PhysRevB.88.155316

[3] Fumani, A. K., & Berezovsky, J. Spin-Pumping Efficiency in Room-Temperature CdSe Nanocrystal Quantum Dots. The Journal of Physical Chemistry C, 118(48), (2014): 28202-28206.

[4] Berezovsky, J., Fumani, A. K., & Wolf, M. Room-temperature initialization, dynamics, and measurement of coherent electron spins in strongly confined quantum dots. In SPIE NanoScience+ Engineering (pp. 916707-916707). International Society for Optics and Photonics (2014).

Changes in research objectives (if any):

Change in AFOSR Program Manager, if any:

Extensions granted or milestones slipped, if any:

AFOSR LRIR Number

LRIR Title

Reporting Period

Laboratory Task Manager

Program Officer

Research Objectives

Technical Summary

Funding Summary by Cost Category (by FY, $K)

	Starting FY	FY+1	FY+2
Salary			
Equipment/Facilities			
Supplies			
Total			

Report Document

Report Document - Text Analysis

Report Document - Text Analysis

Appendix Documents

2. Thank You

E-mail user

Nov 19, 2015 09:56:23 Success: Email Sent to: jab298@case.edu